Structural Analysis of the αN-Terminal Region of Erythroid and Nonerythroid Spectrins by Small-Angle X-ray Scattering[†]

Shahila Mehboob,[‡] Jaby Jacob,[§,||] Melissa May,[‡] Leszek Kotula,[⊥] Pappannan Thiyagarajan,[§] Michael E. Johnson,*[,‡] and Leslie W.-M. Fung*[,∇]

Center for Pharmaceutical Biotechnology, University of Illinois at Chicago, 900 South Ashland Avenue, Chicago, Illinois 60607, Argonne National Laboratory, 9700 South Cass Avenue, Argonne, Illinois 60439, Department of Biochemistry and Molecular Biology, University of Chicago, 920 East 58th Street, Chicago, Illinois 60637, Laboratory of Molecular Neurobiology, New York State Institute for Basic Research in Developmental Disabilities, 1050 Forest Hill Road, Staten Island, New York 10314, and Department of Chemistry, Loyola University of Chicago, 6525 North Sheridan Road, Chicago, Illinois 60626

Received August 5, 2003; Revised Manuscript Received September 25, 2003

ABSTRACT: We used SpαI-1−156 peptide, a well-characterized model peptide of the αN-terminal region of erythrocyte spectrin, and SpαII-1−149, an αII brain spectrin model peptide similar in sequence to SpαI-1−156, to study their association affinities with a *β*I-spectrin peptide, Sp*β*I-1898−2083, by isothermal titration calorimetry. We also determined their conformational flexibilities in solution by small-angle X-ray scattering (SAXS) methods. These two peptides exhibit sequence homology and could be expected to exhibit similar association affinities with *β*-spectrin. However, our studies show that the affinity of SpαII-1−149 with Sp*β*I-1898−2083 is much higher than that of SpαI-1−156. Our SAXS findings also indicate a significantly more extended conformation for SpαII-1−149 than for SpαI-1−156. The radius of gyration values obtained by two different analyses of SAXS data and by molecular modeling all show a value of about 25 Å for SpαI-1−156 and of about 30 Å for SpαII-1−149, despite the fact that SpαI-1−156 has seven amino acid residues more than SpαII-1−149. For SpαI-1−156, the SAXS results are consistent with a flexible junction between helix C′ and the triple helical bundle that allows multiple orientations between these two structural elements, in good agreement with our published NMR analysis. The SAXS findings for SpαII-1−149 support the hypothesis that this junction region is rigid (and probably helical) for αII brain spectrin. The nature of the junction region, from one extreme as a random coil (conformationally mobile) segment in αI to another extreme as a rigid segment in αII, determines the orientation of helix C′ relative to the first structural domain. We suggest that this particular junction region in α-spectrin plays a major role in modulating its association affinity with *β*-spectrins, and thus regulates spectrin tetramer levels. We also note that these are the first conformational studies of brain spectrin.

After first being identified in erythrocytes (*1*), several spectrin isoforms have since been discovered. In humans, two α-spectrins (SpαI and SpαII),[1] four *β*-spectrins (Sp*β*I, Sp*β*II, Sp*β*III, and Sp*β*IV), and a *β*-H spectrin have been sequenced (*2*). αIΣ1 (GenBank accession no. J05244) and *β*IΣ1 (GenBank accession no. J05500) are both found in erythrocytes. αIΣ1*β*IΣ1 (often simplified as αI*β*I) is often referenced as erythroid spectrin. αIIΣ1 (GenBank accession no. XP026977) and *β*IIΣ1 (GenBank accession no. Q01082) are found in axons. αIIΣ1*β*IIΣ1 is variously referenced as nonerythroid spectrin, brain spectrin, or fodrin.

Each Spα or Sp*β* consists primarily of multiple homologous sequence motifs of ∼106 amino acid residues that presumably fold into a triple α-helical structural domain (*3*−*5*). The structure of a single spectrin structural domain of *Drosophila* spectrin was determined by X-ray crystallography (*6*) and that of chicken brain spectrin by both X-ray crystallography and NMR (*7*−*8*). Their findings support the general model of a triple helical bundle for the structural domains. NMR studies of a recombinant peptide from erythrocyte spectrin show a similar (coiled coils) structural

[†] This work was supported by grants from the NSF and American Heart Association Midwest Affiliate (to L.W.-M.F.), the NIH (to L.K., M.E.J., and L.W.-M.F.), and the Packard Foundation Interdisciplinary Science Program (99-8327) (to P.T.). This research benefitted from the use of an isothermal titration calorimeter at Dr. P. Gettins' laboratory at the University of Illinois at Chicago (funded by a shared instrumentation grant, S10 RR15958, from the National Institutes of Health), of BESSRC-CAT funded by the DOE (BES Chemical Sciences), and of BioCAT funded by the NIH, NCRR, and DOE (BES Material Sciences).

* To whom correspondence should be addressed. (M.E.J.) Phone: (312) 996-9114. Fax: (312) 413-9303. E-mail: mjohnson@uic.edu. (L.W.-M.F.) Phone: (773) 508-3128. Fax: (773) 508-3086. E-mail: lfung@luc.edu.

[‡] University of Illinois at Chicago.

[§] Argonne National Laboratory.

[||] University of Chicago.

[⊥] New York State Institute for Basic Research in Developmental Disabilities.

[∇] Loyola University of Chicago.

[1] Abbreviations: D_{max}, maximum dimension; *I*, scattering intensity; ITC, isothermal titration calorimetry; K_d, dissociation constant; *P*(*R*), distance distribution function; **Q**, scattering vector; R_g, radius of gyration; SAXS, small-angle X-ray scattering; SpαI, erythroid α-spectrin; SpαII, nonerythroid α-spectrin.

10.1021/bi0353833 CCC: $25.00
Published on Web 11/18/2003

SpαI-1-51	MEQFPKETVV ESSGPKVLET AEEIQERRQE VLTRYQSFKE RVAERGQKLE D
SpαII-1-42	M DPSGVKVLET AEDIQERRQQ VLDRYHRFKE LSTLRRQKLE D
SpαI-52-111	SYHLQVFKRD ADDLGKWIME KVNILTDKSY EDPTNIQGKY QKHQSLEAEV QTKSRLMSEL
SpαII-43-102	SYRFQFFQRD AEELEKWIQE KLQIASDENY KDPTNLQGKL QKHQAFEAEV QANSGAIVKL
SpαI-112-156	EKTREERFTM GHSAHEETKA HIEELRHLWD LLLELTLEKG DQLLR
SpαII-103-149	DETGNLMISE GHFASETIRT RLMELHRQWE LLLEKMREKG IKLLQXX

FIGURE 1: Sequence alignment (PredictProtein at www.expasy.ch) of SpαI-1−156 and SpαII-1−149 was done using the tryptophan residues (residue 68 in SpαI-1−156 and residue 59 for SpαII-1−149). The two peptides are about 80% similar and 54% identical in sequence. The residues in SpαII corresponding to residues 52−156 in the first structural domain in SpαI are residues 43−147. We have shown that SpαI-1−156 begins with 20 residues in a random coil conformation. The corresponding region in SpαII-1−149 consists of 11 residues. Helix C′, the partial domain in SpαI involved in the association with SpβI at the tetramerization site, consists of residues 21−45, and the corresponding residues in SpαII-1−149 are residues 12−36.

domain, but also show specific differences in helical length and in interhelical residue interactions (*9*).

SpαI and SpβI associate laterally (side-to-side) to form long heterodimers. Formation of the αβ heterodimers involves a two-step "zipper action" process that involves an initial high-affinity contact of complementary nucleation sites on Spα and Spβ (the last four domains in the αC-terminus and the first four domains in the βN-terminus), followed by full-length Spα/Spβ association (*10*−*12*). Two such heterodimers involve "end-to-end" self-association of Spα and Spβ with the αN-terminus and the βC-terminus of one heterodimer associating with the βC-terminus and the αN-terminus of another heterodimer (Spα/Spβ) to give a pair of such αN/βC associations to form a tetramer. The αN/βC region is often referred to as the tetramerization site. The affinity of the αN/βC tetramerization site association is known to be weaker (in the micromolar range) (*10*) than that of the αC/βN nucleation site association (∼10 nM) (*13*). Many functions of spectrin involve its interaction with other components such as the spectrin−actin interaction, the spectrin−membrane interaction, the spectrin−ion-channel interaction, etc. (*2*). Yet some of the most fundamental functions of spectrin involve spectrin self-association. Spectrin tetramers have been suggested to be cooperatively coupled to membrane assembly, and the assembly is a linkage targeted by many hereditary hemolytic anemias (*14*). Thus, the tetramerization site is an important functional site for most spectrin isoforms.

The most studied spectrin tetramer is that from human erythrocytes, $(\mathrm{Sp\alpha I/Sp\beta I})_2$. Other tetramers such as $(\mathrm{Sp\alpha II/Sp\beta II})_2$ and mixed hybrids $(\mathrm{Sp\alpha I/Sp\beta II})_2$ and $(\mathrm{Sp\alpha II/Sp\beta I})_2$ have also been observed (*15*). There is a sequence homology among the different isoforms at the tetramerization site that led to the suggestion that, at the tetramerization site, the structure−function relationship in one isoform can be extrapolated to those of other isoforms (*7*). Yet the self-association affinity in brain spectrin (SpαII/SpβII) is about 15-fold higher than the affinity in erythrocyte spectrin (SpαI/SpβI) (*16*). It is likely that the mixed hybrids (for example, SpαI/SpβII) also exhibit different affinities.

Many highly homologous proteins with similar general folding patterns exhibit small conformational differences that provide functional variations. Various spectrin isoforms probably consist of key conformational differences in specific regions to provide different functions, and it is crucial to determine these differences to understand association affinities and mechanisms of different spectrin isoforms at the tetramerization site.

Assuming that the Spα and Spβ subunits assemble at two major but independent sites, namely, the dimerization site and the tetramerization site, we focused on the conformations at the N-terminus of SpαI and SpαII to understand their contribution toward the difference in affinities of Spα and Spβ association to form tetramers. We used the SpαI-1−156 peptide, a well-characterized model peptide of the αN-terminal region of erythrocyte spectrin that associates with an SpβI model peptide, SpβI-1898−2083 (*17*), and SpαII-1−149, an SpαII model peptide similar to SpαI-1−156 in sequence, to study their association affinities with the SpβI model peptide by isothermal titration calorimetry (ITC) and their conformations in solution by small-angle X-ray scattering (SAXS) methods. With respect to spectrin tetramerization, SpαI-1−156 and SpαII-1−149 are both functional peptides that lack the dimer nucleation site, thus allowing us to study the weaker tetramerization interactions in the absence of the stronger dimerization interactions. SAXS measurements provide direct access to the shape and dimensions of the peptides. Scattering data are often very sensitive to domain orientation, conformational changes, and/or flexibility (*18*−*20*). SAXS analysis is particularly useful when high-resolution structural information, such as that from NMR or X-ray crystallography, is not yet available. Our ITC and SAXS findings allow us to compare the structure−function relationship of these two Spα isoforms to obtain a better molecular level understanding of their functional differences.

EXPERIMENTAL PROCEDURES

Sequence Alignment. On the basis of sequence homology, and assuming that the tryptophan at residues 68 in SpαI and 59 in SpαII is the conserved tryptophan in the first structural domain in Spα (*21*−*22*), sequence alignment puts residues 43−147 as the first structural domain in SpαII (Figure 1). This sequence alignment result led us to design the model peptide SpαII-1−149.

Spectrin Recombinant Peptides. SpαI-1−156 and SpβI-1898−2083 were prepared as before (*17*, *23*). SpαII-1−149 was prepared with α-fodrin cDNA 5′J and JS1 (*24*) as a template, and specific primers (5′-GAG GGA TCC ATG GAC CCA AGT GGG GTC AAA G-3′, containing *Bam*H1 and *Nco*1 sites, and 5′-AGT GAA TTC TAG ATC ACT GGG CCT GCA GCA ATT TG-3′, containing *Eco*R1 and *Xba*1 sites). The DNA fragment was inserted into the pGEX-2T plasmid using the *Bam*H1 and *Eco*R1 restriction sites. The DNA sequence was verified by sequence analysis.

The peptides SpαI-1−156 and Sp*β*I-1898−2083 were expressed in *Escherichia coli* (*E. coli*) DH5α cells, and SpαII-1−149 was expressed in *E. coli* BL21 cells. The peptides were cleaved by thrombin from GST fusion proteins, following standard laboratory methods (*25*). As part of the thrombin recognition sequence, Gly-Ser remained as the first two residues in all three peptides after thrombin cleavage. Peptide identities were demonstrated by mass spectrometry using electrospray ionization techniques, and the purity from each preparation was checked by polyacrylamide gel electrophoresis. Protein concentrations were determined with extinction coefficient values (16500 cm^{-1} M^{-1} for SpαI-1−156, 15220 $cm^{-1}M^{-1}$ for SpαII-1−149, and 31010 cm^{-1} M^{-1} for Sp*β*I-1898−2083), on the basis of their sequences, using the ProtParam program (http://www.expasy.ch/tools/protparam.html). The helical contents of the peptides were determined by circular dichroism (*17*).

Isothermal Titration Calorimetry. ITC measurements were performed at 25 °C with an isothermal titration calorimeter (VP ITC, MicroCal, LLC, Northampton, MA). All peptides were dialyzed with a phosphate buffer (5 mM with 150 mM sodium chloride at pH 7.4) and thoroughly degassed before each titration experiment. Multiple (*15*−*30*) injections, each about 5 μL of SpαI (about 130−340 μM), were introduced into the sample cell containing the Sp*β* peptide (about 9−25 μM). Similar injections (4 μL each) of SpαII peptide (60−120 μM) to the sample cell containing the Sp*β* peptide (about 3−4 μM) were also done. To allow complete equilibrium for the association, the injections were generally carried out with 750 s time intervals (1600 s time intervals were also used to provide adequate isotherm baselines) for the SpαI-1−156 system and 410 s for the SpαII-1−149 system. The first injection point was typically not used due to the loss of sample from the syringe needle to the sample cell.

The heat evolved with each injection was used to measure the dissociation affinity K_d (*26*), using a single-site model of binding provided by the software associated with the ITC instrument (Origin, MicroCal, LLC). The enthalpy of binding in general, or of the association of Spα/Sp*β* peptides in this study, was the heat that must be either added or removed from the reference cell to maintain a constant temperature (*26*). Values for ΔH, ΔS, and ΔG were also obtained from the titration isotherms.

Small-Angle X-ray Scattering Experiments. The peptides (∼2 mg/mL or ∼120 mM) were in 20 mM Tris buffer with 150 mM sodium chloride at pH 7.4. Tris buffer was used for SAXS measurements since the phosphate buffer used in ITC measurements is a poor free radical quencher compared to Tris buffer, and free radicals form due to synchrotron X-rays. Tris buffer was not used for samples used for ITC measurements due to the high heat of buffer ionization, whereas phosphate buffer exhibits a small proton ionization enthalpy. CD measurements of SpαI-1−156 in both buffers showed similar helical contents, about 60%, and of SpαII-1−149 in both buffers also showed similar helical contents, about 70%.

Measurements were carried out at room temperature using the SAXS instrument at the Advanced Photon Source of Argonne National Laboratory. Data were collected using a 15 cm × 15 cm, high-resolution, position-sensitive, nine-element-tiled, CCD mosaic detector at the BESSRC-CAT beam line (*27*), or a 4.9 cm × 8.6 cm CCD area detector at the BioCAT beam line. The sample-to-detector distance was 2.2 m. At the BESSRC beam line (ID-12), 10 successive 1 s exposures were recorded for each sample (in a thermostated quartz capillary flow cell of 1.5 mm diameter) at room temperature, and at the BioCAT beam line (ID-18), five successive 10 s exposures were recorded for each sample. Samples were measured under constant gas flow conditions to reduce potential radiation damage. No evidence of sample changes was seen over the time interval of exposure.

The measurement of each sample was preceded and followed by a measurement of the same buffer solution used in protein sample preparation. These buffer measurements provided a check on beam properties and the cleanliness of the sample cell between sample measurements as well as the means for background subtraction. For the purpose of obtaining data at high angles to generate low-resolution shapes of the peptides using the program GASBOR (see below), the sample-to-detector distance was reduced from 2.2 to 0.8 m. The precision in our experimental procedures, with low protein sample concentrations and small error bars, allowed us to produce data for modeling with GASBOR.

SAXS Data Analysis. Generally, scattering intensities (I) as a function of $\mathbf{Q}$, where $\mathbf{Q}$ is the scattering vector, for SpαI-1−156 and SpαII-1−149 were analyzed with established methods (*18*, *28*, *29*). The radius of gyration, R_g, values were obtained from the Guinier plots, in the range $\mathbf{Q}\cdot R_g \leq 1.3$, where $R_g = [3(\text{slope})]^{1/2}$ and $I_0 = \exp(y\text{-intercept})$ (*18*, *29*).

More precise structural parameters were derived from the distance distribution function, $P(R)$, calculated using the entire scattering profile, up to a $\mathbf{Q}$ of 0.2 A^{-1}. The $P(R)$ function represents the probability of finding a point within the object at a distance R from a given point, and is defined as $4\pi VR^2[\gamma(R)]$, where V is the volume and $\gamma(R)$ is the characteristic function of the particle. Thus, $P(R)$ has a maximum at the most probable distance in the object (e.g., slightly larger than the radius for a sphere) and goes to zero at the maximum dimension, D_{max}, of the object (e.g., the diameter) (*18*). The scattering data were subjected to indirect Fourier transformation using the program GNOM (*30*) to compute the pair distance distribution function $P(R)$. R_g values were also calculated from the second moment of the $P(R)$ functions (*18*, *31*).

SAXS data also carry molecular weight information, and such information provides an indication of sample aggregation state, which may affect data interpretation. To calculate the molecular weight from the SAXS data, the scattering intensity was measured on an absolute scale. A convenient method for obtaining intensity data on an absolute scale is by measuring the scattering intensity of a standard, such as water (*32*). When the intensity data of water are measured on an absolute scale, $I(\mathbf{Q})$ is the same as the angle-independent scattering cross-section ($d\Sigma/d\Omega$), which is proportional to the isothermal compressibility (χ_T), as shown in the equation $d\Sigma/d\Omega = \rho^2 kT\chi_T$, where ρ is the scattering length density, k is Boltzmann's constant, and T is the temperature. We obtained SAXS data for water, using exactly the same configuration, energy, and geometry as for the samples, with $d\Sigma/d\Omega = 1.63 \times 10^{-2}$ cm^{-1} at 293 K (this procedure was used on a regular basis, and the results did not vary beyond the 5% level), and obtained a scale factor by comparing the measured angle-independent data and the expected scattering cross-section. The scattering intensity data of the samples were then multiplied by the scale factor to place them on an absolute scale. The molecular weights of the samples were calculated using the expression $M_w = 10^3 I_0 d^2 N_A / c(\rho_p - \rho_s)^2$, where I_0 (cm^{-1}) is the scattering intensity on the absolute scale (scaled scattering intensity) extrapolated to zero angle, d is the density of the protein (taken as 1.4 gm·cm^{-3}) (*32*), N_A is the Avogadro number, c is the concentration (2 mg/mL), and $\rho_p - \rho_s$ is the scattering length density difference between the peptides (ρ_p) and buffer (ρ_s) (taken as 2.6×10^{10} cm^{-2}) (*32*).

Calculation of R_g Values from a Known Structure and from a Model Structure. Independent of the SAXS data, R_g values were also calculated from structural coordinates with the program CRYSOL (*33*). For SpαI-1−156, coordinates were obtained from NMR studies (*9*, *34*). This structure consists of a lone helix C′ followed by a triple helical bundle structural domain. Since helix C′ is connected to the triple helical bundle with a segment of random coil, it assumes a random distribution of orientations with respect to the triple helical bundle. We estimated the probability distribution for the orientation of helix C′ with respect to the triple helical bundle by considering a sphere with its origin at a point between helix C′ and the triple helical bundle, and with the radial vector defined by helix C′. We defined the polar angle $\theta = 0$ as being the fully extended conformation, with helix C′ extended out from the triple helical bundle in a straight line. Assuming no conformational bias for a specific orientation, we expect to observe helix C′ orientations uniformly distributed over the surface of this sphere. For convenience, we defined equally spaced circles around the sphere defined by the radial vector at constant θ, with θ incremented by a constant value of 10°. For equal spacing of points, each circle would have points spaced at the separation between circles, or $N(\theta) = 2n \sin \theta$ for each θ, where $n = 19$ for 10° increments from 0° to 180°. The probability for finding helix C′ at each angle θ_i was then $N(\theta_i)/\sum N(\theta_i)$.

We generated a model, using the program LSQMAN from the ccp4 suite in the Uppsala Software Factory (http://xray.bmc.uu.se/usf/), for each of the 19 orientations (angles) of helix C′ in SpαI-1−156. The random coil region preceding helix C′ (residues 1−20) was not considered in these models. R_g values were calculated from the coordinates of these 19 models, and each value was then weighted by its corresponding probability value. The sum of the weighted values was then considered to be the calculated R_g value for SpαI-1−156.

For the SpαII-1−149 peptide, since no structural coordinates are available, we used a model in which the junction region connecting helix C′ to the triple helical bundle was helical, and thus, the lone helix C′ was restricted to only one orientation with respect to the triple helical structural domain; i.e., helix C′ extended out from the triple helical bundle in a straight line (Figure 5). We used the backbone coordinates from X-ray studies of the 14th structural domain in *Drosophila* spectrin (*6*), and the side chains of *Drosophila* spectrin were replaced with the corresponding side chains of SpαII-1−149, followed by energy minimization, using Insight II (MSI/Accelerys, San Diego, CA), to generate coordinates for the SpαII-1−149 model for R_g calculations.

Molecular Shape Modeling. A low-resolution molecular shape/envelope model was generated from the measured SAXS data using an ab initio procedure (*19*) and implemented by the program GASBOR. GASBOR uses the higher resolution part of the X-ray scattering pattern ($0.2 < \mathbf{Q} < 0.5$ Å^{-1}) to construct a three-dimensional model, consisting of an assembly of spherical dummy residues, each centered on the Cα position, with a nearest-neighbor distribution constraint to give a random-walk Cα chain. This Cα chain was then folded in such a way as to minimize the discrepancy between the calculated scattering curve from the folded model and the experimental scattering curve. A stable and self-consistent process, consisting of multiple independent runs of ab initio shape determination with no symmetry restriction, was performed for consistent results, as judged by the structural similarity of the output models, nearly identical scattering patterns, and fitting statistics. A low-resolution envelope of the protein was obtained with a final shape restoration, by averaging the shapes from multiple runs using the program DAMAVER (*35*).

RESULTS

Sequence Alignment. Sequence alignment analysis showed that the first 156 residues in SpαI are similar to the first 147 residues in SpαII. Thus, SpαII-1−147 is a SpαII peptide similar to SpαI-1−156. We prepared SpαII-1−149, a peptide with two more amino acid residues at the end than SpαII-1−147. Sequence analysis showed SpαI-1−156 and SpαII-1−147 to be 80% similar and 54% identical (Figure 1). The residues in SpαII corresponding to residues 52−156 in the first structural domain in SpαI (*25*) are residues 43−147. SpαI-1−156 begins with 20 residues in a random coil conformation (*34*). The corresponding region in SpαII-1−149 consists of 11 residues. Helix C′, the partial domain in SpαI that is involved in the association with Spβ I at the tetramerization site (*17*), consists of residues 21−45 (*34*), and the corresponding residues in SpαII-1−149 are residues 12−36. Helix C′ is connected to helix A in the first structural domain by seven amino acid residues (at positions 46−52), in a random coil conformation in SpαI-1−156 (*9*).

Peptide Characterization. We have previously characterized SpαI-1−156 and SpβI-1898−2083 (*17*, *23*). The N-terminal amino acid sequencing analysis confirmed the identity of the first 10 residues of SpαII-1−149, and DNA sequencing confirmed the identity of the codons for SpαII-1−149. In addition, the molecular mass was determined with electrospray ionization mass spectrometry as 17.86 kDa, which was exactly the theoretical value, thus confirming the identities of the amino acid residues in SpαII-1−149. The α-helical content, from CD analysis, was about 60% for SpαI-1−156, 70% for SpαII-1−149, and 60% for SpβI-1898−2083, suggesting that all the peptides were well folded. SDS−PAGE results indicated that the peptides used for the SAXS and ITC experiments were at least 99% pure for SpαI-1−156 and SpαII-1−149, and 95% pure for SpβI-1898−2083.

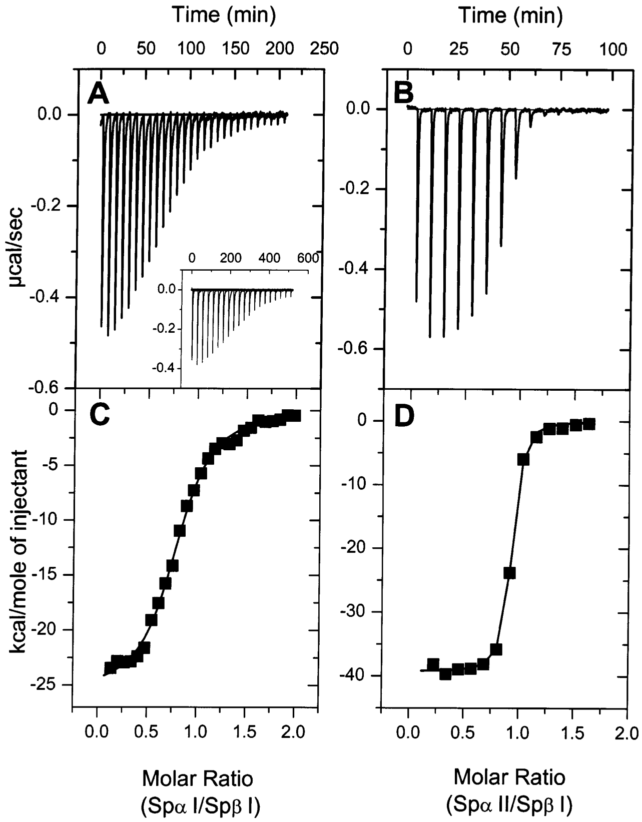

FIGURE 2: Representative raw ITC data for the binding of (A) SpαI-1−156 (340 μM; 5 μL and 750 s time interval per injection) to SpβI-1898−2083 (25 μM, 1.4 mL) and (B) SpαII-1−149 (60 μM; 4 μL and 410 s per injection) to SpβI-1898−2083 (3 μM, 1.4 mL) in PBS pH 7.4 buffer at a temperature of 25 °C. The fitted binding isotherm is shown in (C) for SpαI-1−156 and SpβI-1898−2083 association and in (D) for SpαII-1−149 and SpβI-1898−2083 association. The inset in (A) is that with a 1600 s time interval between injections to demonstrate an adequate baseline for the SpαI-1−156 and SpβI-1898−2083 system.

Isothermal Titration Calorimetry. Analysis of data on heat released upon titration of βI peptide solution with various amounts of α peptide SpαI-1−156 (Figure 2A) or SpαII-1−149 (Figure 2B) gives the Spα/Spβ association isotherms (heat released per mole of α peptide as a function of α peptide molar ratio in solution) for SpαI-1−156 (Figure 2C) and for SpαII-1−149 (Figure 2D). These two isotherms clearly show that the association affinity of SpαI-1−156 and SpβI-1898−2083 differs from that of SpαII-1−149 and SpβI-1898−2083. To ensure that the differences we observed were not artifacts, we varied the concentrations of peptides (130−340 μM for SpαI-1−156 with 9−25 μM for SpβI-1898−2083, and 60−120 μM for SpαII-1−149 with 3−4 μM for SpβI-1898−2083). For the SpαI-1−156 and SpβI-1898−2083 system, we also varied the time intervals between injections to ensure an adequate baseline in the titration isotherm (Figure 2A inset). The K_d values obtained from the isotherms indicate that SpαII-1−149 exhibits much stronger association affinity for SpβI, with a mean K_d value of 0.012 μM, as compared to that of SpαI-1−156, which exhibits a mean K_d value of 1.1 μM (Table 1). The K_d value obtained from the incomplete isotherm (experiment terminated after 10 h due to sample stability) with an injection time interval of 1600 s (Figure 2A inset) was about 0.9 μM. This value was not used due to the incomplete titration.

Table 1: Thermodynamic Parameters Derived from ITC Data for the Association of SpαI-1−156 or SpαII-1−149 with SpβI-1898−2083[a]

sample	K_d (μM)	ΔG (kJ/mol)	ΔH (kJ/mol)	ΔS (J/mol/deg)
SpαI-1-156	1.1 ± 0.1[b]	−34.0 ± 0.3	−115.0 ± 12.3	−272.0 ± 40.5
SpαII-1-149	0.012 ± 0.007	−45.5 ± 1.6	−160.7 ± 4.9	−386.6 ± 11.6

[a] The experiment was carried out at 25 °C in PBS pH 7.4 buffer. The values are the mean values ± standard deviation (s_{n-1}) with n = 2. [b] The calculated statistical uncertainty for K_d values is about 10−15%, with χ^2 values of $10^{5-}10^6$. The measurement reproducibility for K_d is about 10% for the SpαI-1−156 system and about 60% for the SpαII-1−149 system.

The titration curve of SpαII (Figure 2D) is rather steep, indicating strong affinity, similar to others reported for K_d values in the nanomolar range (*36*). Due to ITC sensitivity, an amount of about 2 × 10^{-10} mol per injection is needed for adequate signal intensity, thus limiting the resolution in the titration curve. However, the χ^2 values for the SpαII-1−149 fits were similar to those for SpαI-1−156, both of which were in the $10^{5-}10^6$ range, indicating reliable values for K_d. In addition, the inflection points of the isotherms in Figure 2C,D showed that the stoichiometries (molar ratios) for the associations were around 1, providing validity to the single-site model used in obtaining K_d values.

The different association affinities were due to differences in both the enthalpy change (ΔH) and entropy change (ΔS). Generally, enthalpy changes are primarily due to changes in the interactions (i.e., van der Waals, H-bond, and electrostatic interactions), while entropy changes are primarily due to solvation and conformational entropy effects. Both ΔH and ΔS values for SpαII-1−149 association with βI peptide are more negative than those for SpαI-1−156 association with the β peptide, but with ΔH dominating to generate a more favorable ΔG, by about 12 kJ/mol, for SpαII-1−149 and βI association.

Small-Angle X-ray Scattering. The measured SAXS profiles (Figure 3A) showed clear differences between SpαI-1−156 and SpαII-1−149 peptides. Since the SAXS profile is sensitive to the size, shape, and internal density distribution of a scattering molecule (*37*), the differences in the profiles can be attributed to differences in conformations between the two peptides.

A simple way to illustrate the differences in the conformation of the peptides from the SAXS data is through the Kratky plot, wherein $I(\mathbf{Q})\cdot\mathbf{Q}^2$ is plotted as a function of **Q** (Figure 3B). Generally, the $I(\mathbf{Q})\cdot\mathbf{Q}^2$ values in the Kratky plot provide a measure for the compactness of the scattering particles; the lower the maximum values, the more extended the conformation for the scattering particles (*38*). The Kratky plot exhibits a plateau at the high **Q** region for scattering particles with extended conformations, since the Debye function for scattering intensity from a Gaussian coil has a limiting behavior of $\mathbf{Q}^{-2}$ at high **Q**. However, $I(\mathbf{Q})\cdot\mathbf{Q}^2$ values will decrease at high **Q** for globular/compact particles, for which $I(\mathbf{Q})$ should vary as $\mathbf{Q}^{-4}$. Thus, the $\mathrm{I}(\mathbf{Q})\cdot\mathbf{Q}^2$ values, especially at high **Q**, are related to the shapes of the scattering particles. The Kratky plots for SpαI-1−156 and SpαII-1−149 clearly suggest that SpαII-1−149, with a lower amplitude at low **Q** and longer plateau/higher $\mathrm{I}(\mathbf{Q})\cdot\mathbf{Q}^2$ values at high **Q**, has a relatively more extended structure than SpαI-1−156. In addition, the $\mathrm{I}(\mathbf{Q})\cdot\mathbf{Q}^2$ values of both SpαI-1−

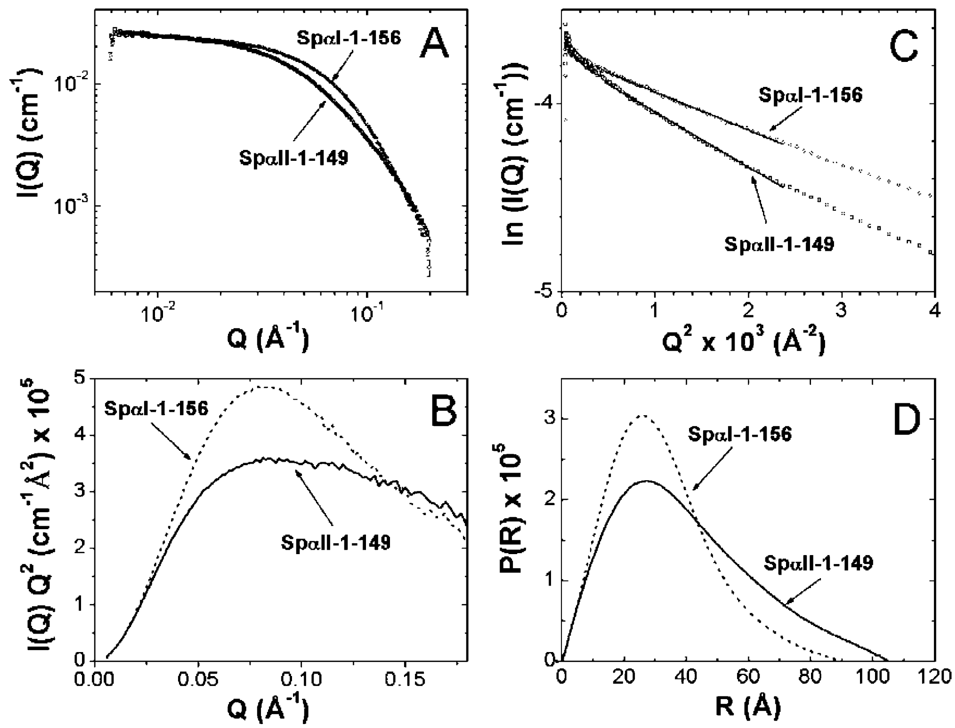

FIGURE 3: SAXS data for the two peptides SpαI-1−156 and SpαII-1−149 at room temperature. The peptides (about 120 μM) were in 20 mM Tris buffer with 150 mM sodium chloride at pH 7.4. (A) The solid line represents the best fit to the experimental data for extracting the $P(R)$ functions in (D); representative statistical errors are shown on the experimental data points. (B) Kratky plots of the SAXS data in (A), with the shift in peak position in SpαII-1−149 relative to that of SpαI-1−156, suggesting that SpαII-1−149 has a relatively more expanded structure than SpαI-1−156. (C) Guinier plots of the SAXS data for the SpαI-1−156 and SpαII-1−149 peptides. Data points in the linear Guinier region (4×10^{-4} Å^{-2} < $\mathbf{Q}^2$ < 2.4×10^{-3} Å^{-2} with a solid line fitted to these points as shown) were used to calculate the R_g values (from the slope of the plots in the region where $\mathbf{Q}\cdot R_g \leq 1.3$). (D) Distance distribution function $P(R)$ calculated from the experimental scattering data in (A). The $P(R)$ function was derived by using the program GNOM (30) to fit the entire scattering data.

Table 2: Parameters Derived from Guinier and $P(R)$ Analysis of SAXS Data[a]

sample	R_g (Å) Guinier	R_g (Å) $P(R)$ analysis	R_g (Å) model	D_{max} (Å)	molecular weight (kDa) Guinier	molecular weight (kDa) sequence
SpαI-1-156	24.5 ± 0.1	24.3 ± 0.8	24.1	90	17.6 ± 1.2	18.5
SpαII-1-149	29.4 ± 0.3	30.8 ± 0.9	30.2	105	16.2 ± 0.8	17.9

[a] SAXS experiments were carried out at room temperature on samples of about 2 mg/mL in 20 mM Tris buffer with 150 mM NaCl at pH 7.4. The values are the mean values ± standard deviation (s_{n-1}) with $n = 2$. Both sets of D_{max} values were the same. The molecular weights calculated from the sequence of each peptide are also shown for comparison.

156 and SpαII-1−149 converge toward zero at low **Q**, indicating that the samples were monomeric, and not aggregated.

A more quantitative representation of the difference in conformations can be obtained from the Guinier (ln[I(**Q**)] versus **Q**^{2}) plots. The Guinier plots of the SAXS data for both SpαI-1−156 and SpαII-1−149 (Figure 3C) exhibit a linear region in the low **Q** region. The radius of gyration (R_g), defined as the root-mean-square distance of all elemental volumes from the center of mass of the particle, obtained from the low **Q** region (0.02 Å^{-1} < **Q** < 0.05 Å^{-1}) of the Guinier plots is 24.5 Å for SpαI-1−156 and 29.4 Å for SpαII-1−149 (Table 2). These values provide a quantitative comparison of the spatial extension of these two peptides. SpαI-1−156, a peptide with seven more amino acid residues, has an R_g value about 20% smaller than that of SpαII-1−149. The difference in the R_g values of the peptides must be due to the difference in their tertiary structures, and not due to different aggregation states in the two peptides, since the samples were shown by the Kratky plots to be monomeric. In addition, the molecular weight analysis from the I_0 values at the y-intercept of the fits in the Guinier plots showed that the molecular weights for SpαI-1−156 and SpαII-1−149 were within 10% of the expected molecular masses of the peptides in monomeric form (Table 2), further indicating the absence of any aggregation in the solutions of the samples.

Another method that provides quantitative evaluation of the conformational differences between the peptides is to calculate the distance distribution function $P(R)$. A symmetric bell-shaped curve in the $P(R)$ versus R plot centered at the most probable distance between two points within the molecule is indicative of a symmetric (e.g., spherical) molecule. However, our $P(R)$ profiles obtained from the fits to the SAXS data using the indirect Fourier transform method for both SpαI-1−156 and SpαII-1−149 are asymmetric (Figure 3D), indicating asymmetrically shaped peptides. The curve for SpαII-1−149 is more asymmetric than that for SpαI-1−156. Both $P(R)$ profiles peak around 20 Å. We suggest that these distances correspond to the short intramolecular distances, mainly within the triple helical bundle structural domain (observed for both peptides). The lone helix (helix C′) in SpαI-1−156 exhibits multiple orientations with

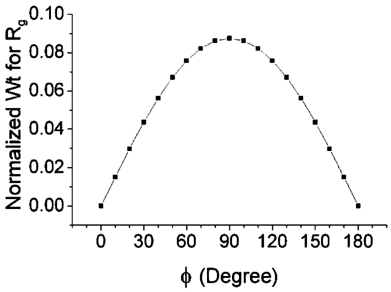

FIGURE 4: Normalized weight used in R_g calculation for SpαI-1−156. It is the probability distribution for the orientation of helix C′ with respect to the triple helical bundle in SpαI-156, as determined by solution NMR studies (*9*). $\theta = 0°$ corresponds to the fully extended conformation, while $\theta = 180°$ corresponds to the folded conformation with helix C′ bundled with the triple helical bundle.

respect to the triple helical bundle. Hence, the distances between helix C′ and the triple helical bundle would vary and thus become effectively lower than the probable distances within the triple helical bundle, such that this distance distribution is masked by the distance distribution profile for the triple helical bundles.

R_g values obtained from the second moment of the $P(R)$ function were very similar to those obtained from the Guinier plots (Table 2). Unlike the Guinier analysis, the $P(R)$ analysis utilizes the SAXS data over the entire **Q** region and provides an alternative estimate of R_g. The consistency between the R_g values obtained from these two independent analyses reflects the excellent quality of the scattering data and the absence of any aggregation in the samples. The $P(R)$ analysis also provides maximum dimension (D_{max}) values for the peptides. The D_{max} values are about 90 Å for SpαI-1−156 and about 105 Å for SpαII-1−149 (Table 2), again indicating that SpαII-1−149 has a significantly larger spatial extension than SpαI-1−156.

R_g values were also calculated from known structures for SpαI-1−156 and from a model structure for SpαII-1−149. The NMR structure for SpαI-1−156 indicates that there is a seven-residue flexible junction between helix C′ and the triple helical bundle (*9*), suggesting that helix C′ will be randomly oriented with respect to the triple helical bundle. The scattering of this molecule will thus result from the ensemble of all orientations. On the basis of a random orientation model for the distribution, Figure 4 shows the estimated probability distribution as a function of the angle between helix C′ and the triple helical bundle. Weighting the calculated $R_g(\theta)$ values (the values ranging from 17.8 to 27.4 Å) by their orientation probabilities gives an average estimated R_g of 24.1 Å, which agrees well with the experimental values (Table 2), validating, on one hand, the methods used to calculate R_g values, and on the other hand, the reliability of the SAXS analysis. Similarly, the R_g value calculated from an extended model structure (Figure 5) for SpαII-1−149 (30.2 Å) agrees well with the experimental values (Table 2), indicating that the structure for SpαII-1−149 probably resembles the model structure that we postulate (Figure 5).

The 10 independent runs of ab initio shape analysis with no symmetry restriction led to consistent results, as judged by the structural similarity of the output models, yielding nearly identical scattering patterns and fitting statistics in a stable and self-consistent process, and produced a molecular

FIGURE 5: Model structure for SpαII-1−149 used for R_g calculation. See the Experimental Procedures section on R_g calculation for model construction.

shape envelope for each peptide (Figure 6). The analysis revealed an elongated shape for the SpαI-1−156 peptide (Figure 6A), but with helix C′ somewhat "compressed", as would be expected if it is averaged over several angular orientations. In addition, the shape for SpαII-1−149 (Figure 6B) was even more extended than that for SpαI-1−156, in good agreement with a larger R_g value for SpαII-1−149. We should point out that this shape analysis does not provide a unique solution, but is one possible solution for interpreting SAXS data.

The schematic representation of SpαII-1−149 presented in Figure 5 shows an extended single helix extending out from the triple helical bundle. The GASBOR representation (Figure 6B) suggests that the two segments may exhibit an average angle of about 30° from a straight line. Comparison of parts A and B of Figure 6 clearly indicates that the erythrocyte peptide exhibits a more compact structure than the brain peptide, consistent with SpαI-1−156 exhibiting conformational averaging.

DISCUSSION

The association of SpαI and SpβI at the tetramerization site has been studied with intact spectrin (*10*, *39*, *40*, *41*) as well as with spectrin fragments (*10*, *17*, *42*−*45*). The association affinity of SpαI-1−156 with the entire β-subunit is weaker ($K_d = 0.3$ μM at 4 °C) than with the β-recombinant peptide ($K_d = 0.14$ μM at 4 °C) (*17*). The 0.3 μM value at 4 °C corresponds to about 10 μM at 30 °C (*45*) and is in good agreement with other studies using recombinant α peptides (*43*, *44*). Helix C′ (residues 21−45) in SpαI is responsible for coiled coil association with the C-terminal partial domain in SpβI (*17*). On the basis of ionic strength and temperature studies (*45*), we have suggested that regions distal to helix C′ as well as structural flexibility and lateral interactions may also play a role in spectrin tetramerization. However, the αN/βC coiled coil association undoubtedly plays a significant role in tetramerization (*17*). Thus, studies with recombinant peptides provide key features in the erythroid spectrin tetramerization process. We have now

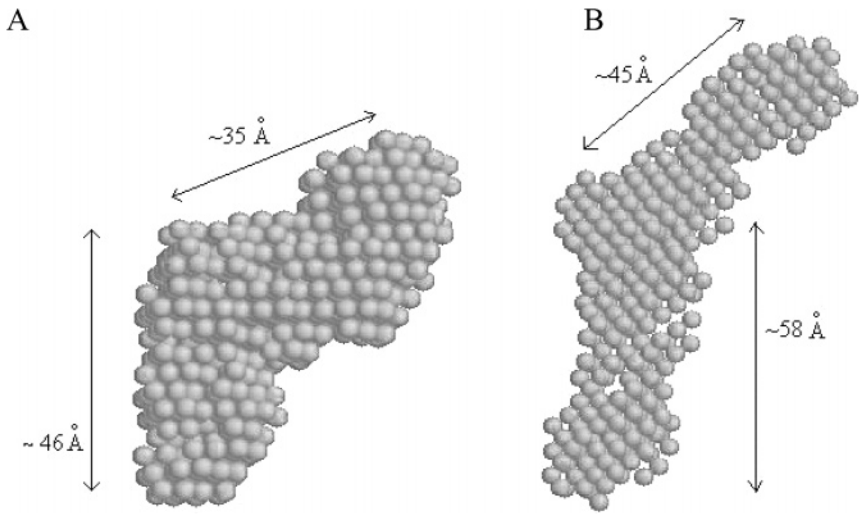

FIGURE 6: Molecular shapes/envelopes determined from the measured SAXS data using an ab initio procedure by the program GASBOR for (A) SpαI-1−156 and (B) SpαII-1−149. All 10 independent runs of ab initio shape analysis with no symmetry restriction lead to consistent results, as judged by the structural similarity of the output models, yielding nearly identical scattering patterns and fitting statistics in a stable and self-consistent process. These models show the peptide SpαII-1−149 to be more elongated than the peptide SpαI-1−156.

extended the studies to nonerythroid spectrin. We show that peptides representing the region consisting of the first 150 or so amino acid residues in SpαI and SpαII, with about 80% similar and 54% identical sequences, exhibit different affinity toward a *β*I peptide, with SpαII-1−149 exhibiting much stronger affinity than SpαI-1−156 toward the *β*I peptide. Our result clearly demonstrates the differences between the αI and αII systems while their *β* partner is held constant.

The molecular shape studies by SAXS methods clearly indicate a more extended conformation for SpαII-1−149 than for SpαI-1−156. The R_g values obtained by two different analyses of SAXS data and by modeling all show values of about 25 Å for SpαI-1−156 and about 30 Å for SpαII-1−149, despite the fact that SpαI-1−156 has seven amino acid residues more than SpαII-1−149. We suggest that SpαI-1−156 exhibits a more flexible conformation than SpαII-1−149 at the junction region linking helix C′ to the first structural domain.

It is often assumed that spectrin flexibility is the molecular origin of the unique deformability and elasticity of erythrocytes (*46*). We and others have shown that intact erythrocyte spectrin exhibits considerable local internal motions (*47*−*54*). These studies suggest that erythrocyte spectrin exhibits segmental motions with a highly flexible region connecting more rigid structural elements. In contrast, it has been suggested that brain spectrin is more rigid than erythrocyte spectrin (*16*).

At present, SpαI is the only spectrin for which the structure of the N-terminal junction region has been determined experimentally (*9*). Early structural prediction studies suggest that helix C_{n-1} of the previous $(n - 1)$th structural domain is connected to helix A_n in the next nth structural domain in Spα by either a *random coil segment* (*3*) or a *helical segment* (*55*). X-ray diffraction studies (*7*) of two-domain peptides, with the sequence from chicken brain Spα, show a *helical linker* linking two domains, with a change in the phasing of the heptad pattern, classified as a “stammer” (*56*). Grum and co-workers further suggest that the erythrocyte spectrin (SpαI) tetramerization site also consists of a *helical junction* (*7*). The SAXS findings for SpαI-1−156 support our NMR results (*9*, *34*), consistent with a *flexible junction* between helix C′ and the triple helical bundle that allows multiple orientations between these two structural elements. The SAXS findings for SpαII-1−149 support the hypothesis that this junction region is rigid (and probably helical) for SpαII brain spectrin. We also note that our SAXS experiment on SpαII-1−149 is the first structural study for the brain spectrin N-terminal region.

We suggest that this helical junction region between helix C′ and helix A_1 in SpαII provides a more rigid orientation for helix C′ than the more flexible orientation observed in SpαI. We further suggest that this particular junction region in Spα plays a major role in modulating its association affinity with Sp*β*, and thus regulates spectrin tetramer levels. The nature of the junction region, from one extreme as a random coil segment in SpαI to another extreme as a helical segment in SpαII, determines the orientation of helix C′ relative to the first structural domain. The potential energy for reorganization of the junction region in SpαI provides a simple mechanism to regulate association of helices A′, B′, and C′ in spectrin. Our ITC data indicate that the affinity difference is due to differences in both the enthalpy change and entropy change. Thus, changes in the van der Waals, H-bond, and/or electrostatic interactions as well as changes due to solvation and/or conformational entropy effects presumably contribute to the higher affinity for SpαII-1−149 association with *β* peptide than for SpαI-1−156 association with *β* peptide. If the junction region is flexible enough to allow helix C′ to interact with the first structural domain, to transiently form a four-helix bundle, a single amino acid mutation in helix C′ or even in the first structural domain may modulate the affinity dramatically (*57*).

An understanding of the structural-association affinity relationship of different spectrin isoforms (αI, αII, *β*I, and *β*II) may provide insight for explaining the various physiological and pathological conditions that are a consequence of varying affinities of Spα and Sp*β* in the self-association to form various spectrin tetramers. Mutations, oxidation, or structural modifications may affect this particular junction conformation and thus cause malfunctioning of spectrin molecules. It has been reported that some spectrin molecules found in erythrocytes of patients with hereditary anemias with mutations in this region exhibit low affinities (*58*). More studies to determine the high-resolution structure of spectrin in this region not only will provide an understanding of some of the diseases but also, more importantly, may point toward therapeutic approaches (*2*), for example, by identifying molecules capable of modifying the conformation and thus the association affinities.

ACKNOWLEDGMENT

We acknowledge the invaluable assistance of Elena Kondrashkina at BioCAT and Soenke Seifert at BESSRC in the SAXS experiments and Klavs Dolmer and Ana Lazic at the University of Illinois at Chicago in the ITC experiments. We also thank Dr. R. T. Moon of the University of Washington School of Medicine and Dr. Vann Bennett of the Duke University Medical Center for the cDNA of brain spectrin and Dr. B. G. Forget of the Yale University School of Medicine for the cDNA of erythrocyte spectrin.

REFERENCES

1. Yu, J., Fischman, D., and Steck, T. L. (1973) *J. Supramol. Struct. 1*, 233−248.
2. Bennett, V., and Baines, A. J. (2001) *Physiol. Rev. 81*, 1353−1392.
3. Speicher, D. W., and Marchesi, V. T. (1984) *Nature 311*, 177−180.
4. Davison, M. D., Baron, M. D., Critchely, D. R., and Wooten, J. C. (1989) *Int. J. Biol. Macromol. 11*, 81−90.
5. Parry, D. A. D., Dixon, T. W., and Cohen, C. (1992) *Biophys. J. 61*, 858−867.
6. Yan, Y. E., Winograd, E., Viel, A., Cronin, T., Harrison, S. C., and Branton, D. (1993) *Science 262*, 2027−2030.
7. Grum, V., Li, D., MacDonald, R., and Mondragon, A. (1999) *Cell 98*, 523−535.
8. Pascual, J., Pfuhl, M., Rivas, G., Pastore, A., and Saraste, M. (1996) *FEBS Lett. 383*, 201−207.
9. Park, S., Caffrey, M., Johnson, M. E., and Fung, L. W.-M. (2003) *J. Biol. Chem. 278*, 21837−21844.
10. Speicher, D. W., DeSilva, T. M., Speicher, K. D., Ursitti, J. A., Hembach, P., and Weglarz, L. (1993) *J. Biol. Chem. 268*, 4227−35.
11. Begg, G. E., Harper, S. L., Morris, M. B., and Speicher, D. W. (2000) *J. Biol. Chem. 275*, 3279−3287.
12. Harper, S. L., Begg, G. E., and Speicher D. W. (2001) *Biochemistry 40*, 9935−9943.
13. Ursitti, J., Kotula, L., DeSilva T. M., Curtis P. J., and Speicher D. W. (1996) *J. Biol. Chem. 271*, 6636−6644.
14. Giorgi, M., Cianci, C., Gallagher, P., and Morrow, J. S. (2001) *Exp. Mol. Pathol. 70*, 215−230.
15. Clark, M. B., Ma, Y., Bloom, M. L., Barker, J. E., Zagon, I. S., Zimmer, W. E., and Goodman, S. R. (1994) *Brain Res. 663*, 223−239.
16. Begg, G. E., Morris, M. B., and Ralston, G. B. (1997) *Biochemistry 36*, 6977−6985.
17. Mehboob, S., Luo, B.-H., Patel, B. M., and Fung, L.W.-M. (2001) *Biochemistry 40*, 12457−12464.
18. Fang, X., Littrell, K., Yang, X.-J., Henderson, S. J., Seifert, S., Thiyagarajan, P., Pan, T., and Sosnick, T. R. (2000) *Biochemistry 39*, 11107−11113.
19. Svergun, D. I., Petoukhov, M. V., and Koch, M. H. J. (2001) *Biophys. J. 80*, 2946−2953.
20. Trewhella, J. (1997) *Curr. Opin. Struct. Biol. 7*, 702−708.
21. Sahr, K. E., Laurila, P., Kotula, L., Scarpa, A. L., Coupal, E., Leto, T. L., Linnenbach, A. J., Winkelmann, J. C., Speicher, D. W., and Marchesi, V. T. (1990) *J. Biol. Chem. 265*, 4434−4443.
22. Winkelmann, J. C., Chang, J. G., Tse, W. T., Scarpa, A. L., Marchesi, V. T., and Forget, B. G. (1990) *J. Biol. Chem. 265*, 11827−11832.
23. Luo, B.-H., Mehboob, S., Hurtuk, M. G., Pipalia, N. H., and Fung, L. W.-M.(2002) *Eur. J. Haematol. 68*, 73−79.
24. Moon, R. T., and McMahon, A. P. (1990) *J. Biol. Chem. 265*, 4427−4433.
25. Lusitani, D. M., Qtaishat, N., LaBrake, C. C., Yu, R. N., Davis, J., Kelley, M. R., and Fung L. W.-M. (1994) *J. Biol. Chem. 269*, 25955−25958.
26. Simonovic, M., Dolmer, K., Huang, W., Strickland, D., Volz, K., and Gettins, P. (2001) *Biochemistry 40*, 15127−15134.
27. Seifert, S., Winans, R. E., Tiede, D. M., and Thiyagarajan, P. (2000) *J. Appl. Crystallogr. 33*, 782−784.
28. Receveur, V., Czjzek, M., Schulein, M., Panine, P., and Henrissat, B. (2002) *J. Biol. Chem. 277*, 40887−40892.
29. Guinier, A., and Fournet, G. (1955) *Small angle scattering of X-rays*, John Wiley and Sons, New York.
30. Svergun, D. I. (1992) *J. Appl. Crystallogr. 25*, 495−503.
31. Heidorn, D., and Trewhella, J. (1988) *Biochemistry 27*, 909−915.
32. Orthaber, D., Bergmann, A., and Glatter, O. (2000) *J. Appl. Crystallogr. 33*, 218−225.
33. Svergun, D. I, Barberato, C., and Koch, M. H. J. (1995) *J. Appl. Crystallogr. 28*, 768−773.
34. Park, S., Johnson, M. E., and Fung, L. W.-M. (2000) *FEBS Lett. 485*, 81−86.
35. Aparicio, R., Fischer, H., Scott, D., Verschueren, K., Kulminskaya, A., Eneiskaya, E., Neustroev, K., Craievich, A., Golubev, A., and Polikarpov, I. (2002) *Biochemistry 41*, 9370−9375.
36. Randall, L., Topping, T. B., Suciu, D., and Hardy, S. J. S. (1998) *Protein Sci. 7*, 1195−1200.
37. Glatter, O., and Kratky, O., Eds. (1982) *Small-Angle X-ray Scattering*, Academic Press, London.
38. Shi, L., Kataoka, M., and Fink, A. L. (1996) *Biochemistry 35*, 3297−3308.
39. Henniker, A., and Ralston, G. B. (1994) *Biophys. Chem. 52*, 251−258.
40. Ralston, G. B. (1991) *Biochemistry 30*, 4179−4192.
41. Tse, W. T., Lecomte, M. C., Costa, F. F., Garbarz, M., Feo, C., Boivin, P., Dhermy, D., and Forget, B. G. (1990) *J. Clin. Invest. 86*, 909−916.
42. Speicher, D. W., Weglarz, L., and DeSilva, T. M. (1992) *J. Biol. Chem. 267*, 14775−14782.
43. DeSilva, T. M., Peng, K. C., Speicher, K. D., and Speicher, D. W. (1992) *Biochemistry 31*, 10872−10878.
44. Kotula, L., DeSilva, T. M., Speichr, D. W., and Curtis, P. J. (1993) *J. Biol. Chem. 268*, 14788−14793.
45. Cherry, L., Menhart, N., and Fung, L. W.-M. (1999) *J. Biol. Chem. 274*, 2077−2084.
46. Vertessy, B. G., and Steck, T. L. (1989) *Biophys. J. 55*, 255−262.
47. Fung, L. W.-M., Soo Hoo, M. J., and Meena, W. A. (1979) *FEBS Lett. 105*, 379−383.
48. Lemaigre-Dubreuil, Y., Henry, Y., and Cassoly, R. (1980) *FEBS Lett. 113*, 231−234.
49. Fung, L. W.-M., and Johnson, M. E. (1983) *J. Magn. Reson. 51*, 233−244.
50. Dubreuil, Y. L., and Cassoly, R. (1983) *Arch. Biochem. Biophys. 223*, 495−502.
51. Fung, L. W.-M., Lu, H. Z., Hjelm, R. P., Jr., and Johnson, M. E. (1986) *FEBS Lett. 197*, 234−238.
52. Learmonth, R. P., Woodhouse, A. G., and Sawyer, W. H. (1989) *Biochim. Biophys. Acta 987*, 124−128.
53. Clague, M. J., Harrison, J. P., and Cherry, R. J. (1989) *Biochim. Biophys. Acta 981*, 43−50.
54. Budzynski, D. M., Benight, A. S., LaBrake, C. C., and Fung, L. W.-M. (1992) *Biochemistry 31*, 3653−3660.
55. Dubreuil, R. R., Byers, T. J., Sillman, A. L., Bar-Zvi, D., Goldstein, L. S., and Branton, D. (1989) *J. Cell Biol. 109*, 2197−2205.
56. Brown, J. H., Cohen, C., and Parry, D. A. (1996) *Proteins 26*, 134−145.
57. Park, S., Johnson, M. E., and Fung, L. W.-M. (2002) *Blood 100*, 283−288.
58. Delaunay, J., and Dhermy, D. (1993) *Sem. Hematol. 30*, 21−33.

BI0353833